Fuel 124 (2014) 221–231

Contents lists available at ScienceDirect

Fuel

journal homepage: www.elsevier.com/locate/fuel

Techno-economic analysis of chemical looping combustion with humid air turbine power cycle

Akeem K. Olaleye, Meihong Wang *

Process and Energy Systems Engineering Group, School of Engineering, University of Hull, Cottingham Road, Hull HU6 7RX, United Kingdom
Process Systems Engineering Group, School of Engineering, Cranfield University, Bedfordshire MK43 0AL, United Kingdom

HIGHLIGHTS

- Process simulation for chemical looping combustion (CLC) and its model validation.
- Process simulation of humid air turbine (HAT) for power generation.
- Process simulation and analysis of CLC–HAT cycle.
- Economic analysis of the CLC–HAT cycle for natural gas-fired power plant with CO_2 capture.
- Comparison between CLC–HAT cycle and conventional HAT cycle.

ARTICLE INFO

Article history:
Received 27 November 2013
Received in revised form 14 January 2014
Accepted 3 February 2014
Available online 15 February 2014

Keywords:
Chemical looping combustion
Humid air turbine
Economic analysis
Process simulation
CO_2 capture

ABSTRACT

Power generation from fossil fuel-fired power plant is the largest single source of CO_2 emission. CO_2 emission contributes to climate change. On the other hand, renewable energy is hindered by complex constraints in dealing with large scale application and high price. Power generation from fossil fuels with CO_2 capture is therefore necessary to meet the increasing energy demand, and reduce the emission of CO_2. This paper presents a process simulation and economic analysis of the chemical looping combustion (CLC) integrated with humid air turbine (HAT) cycle for natural gas-fired power plant with CO_2 capture. The study shows that the CLC–HAT including CO_2 capture has a thermal efficiency of 57% at oxidizing temperature of 1200 °C and reducer inlet temperature of 530 °C. The economic evaluation shows that the 50 MW_{th} plant with a projected lifetime of 30 years will have a payback period of 7 years and 6 years for conventional HAT and CLC–HAT cycles respectively. The analysis indicates that CLC–HAT process has a high potential to be commercialised.

1. Introduction

1.1. Background

Fossil fuels are burned in power plants in a variety of ways. The combustion of fossil fuels produces flue gas stream (i.e. NO*x*, CO_2, SO*x*, CO, CH_4, and water vapour, etc.) with a CO_2 content of up to 14 vol% [1]. CO_2 is the largest and most important anthropogenic greenhouse gas (GHG) [2]. However, fossil fuel fired power plants play a key role in meeting energy demands. With growing concerns over the increasing atmospheric concentration of anthropogenic greenhouse gases, effective CO_2 emission abatement strategies are required to combat this trend [3]. In a fossil fuel-based power plant, CO_2 management is made up of three steps namely CO_2 capture (including separation and compression); transportation and storage [4]. There are three approaches for capturing CO_2 from use of fossil fuels and/or biomass for heat and power generation: pre-combustion, post-combustion and oxy-fuel process [5]. CLC is a relatively new CO_2 capture mechanism. The fuel is converted by its reaction with oxygen from an oxygen carrier rather than air (as in oxy-fuel and pre-combustion). CLC also enables the production of a concentrated CO_2 stream without the need for an expensive air separation unit [6]. The inherent CO_2 separation without severe energy penalties in the CLC process has drawn increased attention in light of power plant efficiency improvement and global warming potential due to fossil fuel combustion [4].

* Corresponding author at: Process and Energy Systems Engineering Group, School of Engineering, University of Hull, Cottingham Road, Hull HU6 7RX, United Kingdom. Tel.: +44 1482 466688.
E-mail addresses: A.K.Olaleye@2012.hull.ac.uk (A.K. Olaleye), Meihong.Wang@hull.ac.uk (M. Wang).

http://dx.doi.org/10.1016/j.fuel.2014.02.002
0016-2361/

Nomenclature

NCV	net calorific value (J/kg)
P	power output (MW)
NPV	net present value (£)
IRR	internal rate of return (%)
η_{ref}	efficiency of Conventional HAT cycle (%)
η_{ccs}	efficiency of HAT cycle with carbon capture (%)
W_{comp}	compressor work (MW)
Q	energy (MW)

Greek symbols

γ	yield
η	efficiency

Subscripts

comp	compressor
ccs	carbon capture and storage
ref	reference
GT	gas turbine
th	thermal

Acronyms

ASU	air separation unit
CFB	circulating fluidized bed
CLC	chemical looping combustion
CLC–HAT	chemical looping combustion with humid air turbine cycle
HAT	humid air turbine
PI	profitability index

1.2. Chemical looping combustion (CLC)

1.2.1. CLC concept

CLC is a method characterised by indirect fuel combustion because the air and fuel are never in direct contact. CLC differs from the oxy-fuel combustion strategy because of the concept of oxygen separation from air and the direct contact of pure oxygen and fuel in the latter [4]. In oxy-fuel combustion, the operation of air separation unit (ASU) accounts for nearly three quarters of overall efficiency loss [7].

Fig. 1 shows a schematic diagram of the CLC concept. The fossil fuel conversion is achieved in two sub-reactions (oxidation and reduction) and with oxygen carrier particle as the chemical intermediates. In the reduction stage, the oxygen carrier particle is reduced by the fuel, yielding CO_2 and H_2O. This is depicted in reaction (1) for a gaseous fuel [4]

$$(x + y/4)\ \mathrm{MeO} + \mathrm{C}_x\mathrm{H}_y \rightarrow (x + y/4)\ \mathrm{Me} + x\mathrm{CO}_2 + y/2\mathrm{H}_2\mathrm{O} \quad (1)$$

This fuel conversion step could either be exothermic or endothermic depending upon the type of oxygen carrier and fuel used. The reduced metal is then sent to the oxidizer where combustion occurs with air. The reduced metal is regenerated to its initial oxidation state as shown in reaction (2) [4].

$$\mathrm{Me} + \mathrm{Air} \rightarrow \mathrm{MeO} + \mathrm{Oxygen\text{-}depleted\ Air} + \mathrm{Heat} \quad (2)$$

The oxidation step being exothermic produces an enormous amount of heat which is used to generate electricity; also the fact that both the fuel and the air conversion process occur in different reactors leads to the production of a CO_2 stream from the reducer that has only H_2O as the other component, hence it is easily separated from the mixture. CLC can be applied to both gaseous (natural gas) and solid fuels (coal) [4].

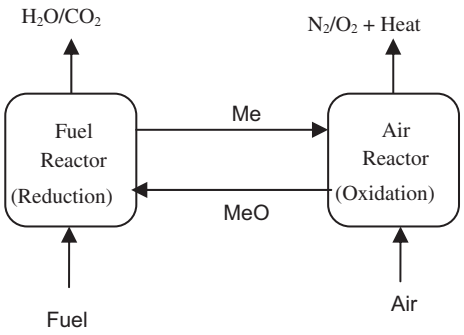

Fig. 1. Schematic of the CLC concept [4].

1.2.2. Review on CLC study

The most common metals used as oxygen carrier include Fe, Ni, and Cu. A number of promising oxygen carriers have been found, of which $NiO/NiAl_2O_4$ is perhaps the most promising [8,9]. NiO/Ni oxygen carrier particle with $NiAl_2O_4$ as inert support material will be used as the oxygen carrier particle in this study. A brief outline of some of the published work on oxygen carrier development is summarized in Table 1.

Reactor design is another important area in CLC development that has witnessed rapid growth. Optimized reactor design is required in order to render the CLC operation economically feasible. Two key factors that dictate the selection of gas–solid reactor are the type of metal oxide carriers employed for the looping operation and the type of products to be produced [4]. Fluidized beds systems have been widely applied for CLC reactor systems modelling, design and experimentation. From the pioneering work of Lyngfelt et al. [17], a number of study are available e.g. [18–20], etc. on the modelling, design and scale-up of fluidized bed reactor system for a successful operation of CLC systems.

1.2.3. CLC power cycles

In order to fully appreciate the gains of a relatively new technology such as CLC, it is imperative to carry out detailed study of its power generation potential. The CLC system can be integrated into different power cycles, and analysed at different operating conditions. These studies are done by modelling and simulation of the power plants with CLC, performing sensitivity analysis for various plant configurations in order to estimate the plant efficiency.

A number of articles have been published on the integration of CLC into power cycles. Different approaches have been adopted at different periods by different researchers to evaluate the potentials of CLC power generation scheme. Two important aspects, however dominates the researches carried out so far, these are;

- Power cycle analysis which focuses mainly on the comparative studies of different power cycles, and
- Exergy analysis of CLC power cycle and its comparison with that of conventional power cycle.

Articles focusing on the first aspect include [21–23], etc. [21–23] made use of a common fuel (CH_4) and similar oxygen carrier

Table 1
Oxygen carrier development.

Authors	Carriers/stabilizers	Fuel/reactant gases	Issues/results
Johansson et al. [10]	$NiO–Fe_2O_3$	CH_4	Using mixed Fe and Ni oxides for CH_4 combustion. Less bed material used with mixed oxides as against Fe only.
Jerndal et al. [11]	Metal oxides based on Ni, Cu, Fe, Mn	CH_4, CO and H_2	Thermal analysis of the CLC process using different O_2 carrier
Abad et al. [12]	Fe_2O_3/Al_2O_3	CH_4/syngas	Low attrition, and particles have high durability, but better suited for syngas than CH_4
Zhao et al. [13]	$NiO/NiAl_2O_4$	Coal char/H_2	$NiO/NiAl_2O_4$ reacts rapidly with coal char at temperature higher than 850 °C with NiO mass content of 60% and sintering temperature of 1300 °C
Abad et al. [14]	$FeTiO_3/TiO_2$	CH_4, CO/H_2	Kinetics of the REDOX reaction were obtained
Mendiara et al. [15]	Bauxite waste (BW)	Coal	Investigates influence of temperature on coal conversion
Mattison et al. [16]	$NiO/NiAl_2O_4$	CH_4	The particles show high rate of reduction with CH_4 in the temperature range 750–950 °C

with different power cycles for comparison. It was found that the cycles integrated with CLC have minute energy losses and CO_2 was separated at a higher capture level. Articles that focus on the exergy analysis include [24,9]. It was reported that the exergy losses in the CLC power cycle were lower compared to conventional cycles.

Authors of [24,9] used the humid air turbine (HAT) power cycle. The HAT cycle is adopted in this research due to its advantages and high thermal efficiency [25]. In this principle, a humidifying tower is used to saturate the incoming air, before combustion [9].

1.3. Aim of this paper and its novel contribution

In this paper, the CLC system is integrated into a HAT cycle. The paper presents a process simulation and economic analysis of CLC in the HAT cycle. The differences between this paper and previous CLC with HAT power cycle reports such as [24,9] are: (a) this paper uses a modular-based simulation tool (Aspen Plus®) with well-defined physical and thermodynamic properties of the reacting species and inert in its database; (b) this paper use a promising oxygen carrier, NiO and $NiAl_2O_4$ as the looping media in modelling and simulation of the CLC process; (c) this paper presents the simulation and process analysis of both the conventional HAT power cycle and CLC–HAT cycle, and (d) this paper carried out economic analysis of the CLC–HAT cycle in order to determine its feasibility, and compare it with equivalent conventional HAT cycle.

2. Simulation of CLC

This section describes the development of CLC simulation in Aspen Plus®. It requires specific skills such as accurate description of property packages of pure components and complex mixtures, models for different types of reactors and unit operations.

2.1. Simulation data for CLC

There exists no full-scale commercial CLC plant (e.g. above 50 MW_{th}). Hence, it is difficult to get a single source with all the necessary information required for the simulation of the CLC based HAT power cycle. The simulation data used in this study were obtained from two different sources [24,9]. The oxygen carrier used in this study; however is $NiO/NiAl_2O_4$ as against NiO with yttrium stabilized zirconium (NiO/YSZ) used by both [24,9].

2.2. Simulation of CLC in Aspen Plus®

The circulating fluidized bed (CFB) reactor is simulated in this paper as a combination of simple RGIBBS and RSTOIC reactor models in Aspen Plus® because most commercial tools do not yet offer a possibility for treatment of gas-solid reactions as needed for CLC

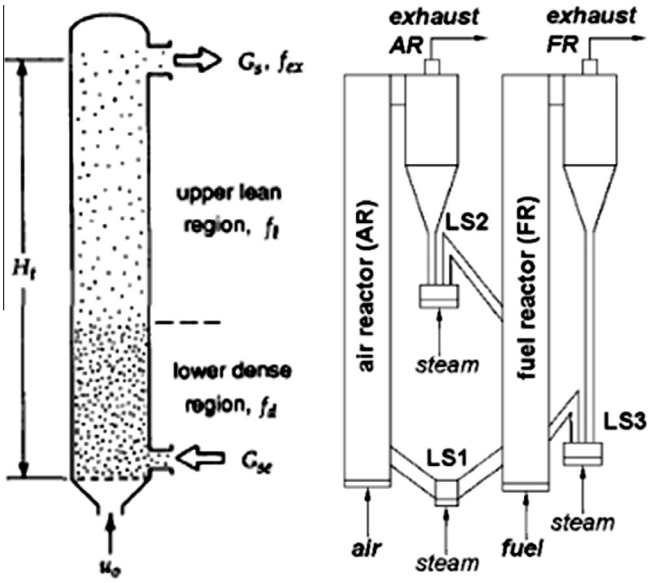

Fig. 2. Typical structure of fluidized bed reactor. (a) [28] and (b) [4].

(i.e. CFB). This approach is similar to that adopted by [4] for simulating syngas chemical looping process for production of electricity, hydrogen and CO_2 capture [4].

2.2.1. Assumptions

- The simulation considers that the CFB is divided into two regions; (a) dense lower region, and (b) a more dilute upper region (Fig. 2(a)).
- Equilibrium based thermodynamic reactions are assumed in the dense region. Products discharged from the reactors are based on minimisation of Gibbs free energy principle, hence the use of RGIBBS module in Aspen Plus®.
- The dilute region is assumed to be in a completely well mixed condition. A stoichiometric reactor module RSTOIC is used.
- The hydrodynamic parameters of the bed and physical properties of the components are considered to be constant throughout the bed.
- The oxidation reaction temperature within the catalytic bed is assumed constant by continuously removing heat at a rate proportional to the temperature difference.
- The reduction (endothermic) depends on the exothermic heat energy from the remooxidizer to operate.

Table 2
Reactions considered in the simulation [27].

Reaction		Reactor
$CH_4 + 2NiO \rightleftharpoons CO_2 + 2H_2 + 2Ni$	(3)	Reducer
$CH_4 + NiO \rightleftharpoons CO + 2H_2 + Ni$	(4)	Reducer
$CO + NiO \rightleftharpoons CO_2 + Ni$	(5)	Reducer
$H_2 + NiO \rightleftharpoons H_2O + Ni$	(6)	Reducer
$4Ni + 2O_2 \rightleftharpoons 4NiO + heat$	(7)	Oxidizer

There are different types of fuels that can be used as feedstock for the CLC operation. This study considers natural gas as feedstock (with 100% CH_4 assumption). The CH_4 in the reducer was converted to CO_2 and H_2O using NiO as oxygen carrier. The NiO is reduced to Ni. $NiAl_2O_4$ plays the role of keeping the mechanical strength of the particle [26]. The reactions considered in this simulation are summarized in Table 2.

2.2.2. Operating conditions of the CLC reactors

The operating parameters and components (mainly reactants) of the CLC reactors are given in Table 3. Fig. 3 is the flowsheet in Aspen Plus® of the dual CFB for the CLC system. When the reducer is operated at 700 °C, the CLC simulation results are presented in Table 4. The results show that with NiO-based carrier particle, a conversion of CH_4 of over 99% can be achieved in the reducer.

2.3. Validation of the CLC simulation

The works of [24,9] do not include analysis of the thermodynamic gas yield and conversions of the gas and solid species in the CLC reactors. The thermodynamic gas yield and, H_2 and CO concentrations for the CH_4 over the $Ni/NiAl_2O_4$ was validated from the experimental results of [29]. This is necessary to analyse and mitigate the thermodynamic limitation of NiO to convert all the CH_4–CO_2 and H_2O at different operating temperatures. The CH_4 conversion and CO_2 yield from the reducer are evaluated from the simulation results thus;

$$\gamma_{CO_2} = \frac{x_{CO_2}}{x_{CH_4} + x_{CO_2} + x_{CO}} \tag{3}$$

$$(1 - X_{CH_4}) = \frac{x_{CH_4}}{x_{CH_4} + x_{CO_2} + x_{CO}} \tag{4}$$

γ_{CO_2}, yield of CO_2; x_i, volume fraction of species i; and $(1 - X_{CH_4})$, conversion of CH_4. The CH_4 conversion and CO_2 yield from the reducer were estimated from Eqs. (3) and (4) as 98.93% and 96.23% respectively. The results in Table 5 shows reasonable agreement with experimental results presented in [29]. A further analysis of the CLC system is explained in Section 2.4.

Table 3
Input streams of the CLC reactors.

Oxidizer	Air		Oxygen carrier	
Species	O_2	N_2	Ni	$NiAl_2O_4$
Flow rates (kg/s)	49.8		37.05	
concentration	21 vol%	79 vol%	40 wt.%	60 wt.%
Temperature (°C)	530		530	
Pressure (bar)	20	20	20	
Reducer	**Fuel**		**Oxygen carrier**	
Species	CH_4		NiO	$NiAl_2O_4$
Flow rates (kg/s)	1.0		32.6	
Mass fraction	100 wt.%		45.9 wt.%	54.1 wt.%
Temperature (°C)	700		1200	
Pressure (bar)	20		20	

2.4. Process analysis for the CLC system

2.4.1. Effect of fuel flow on oxidizer and reducer outlet temperature

Fig. 4 shows the effect of fuel flow rate (kg/s) on the outlet temperatures of the oxidizer and reducer. Due to the reactions in the reducer being endothermic, increasing the flow rate of the fuel (CH_4) decreases the reactor temperature (Fig. 4). This increase in fuel flow in the reducer aids the conversion of NiO–Ni, and increases the availability of Ni for the oxidation reaction in the oxidizer. This increases the rate of oxidation (exothermic) reaction and thus the temperature in the oxidizer. Increasing the fuel flow rate above the stoichiometric amount has no effect on the production of Ni metal. Therefore, after reaching the maximum value (approximately 1200 °C), further increase in fuel flow has no impact on the oxidation reactor temperature.

2.4.2. Effect of humid air/fuel ratio on gas product yield

The effect of the humid air/fuel molar ratio on the product distribution in the fuel reactor was considered in this case study. Fig. 5 shows the gas products CO_2, H_2 and CO concentrations at the reducer outlet. It is observed that increasing the humid air/fuel ratio between 0.8 and 1.2 and reactor temperature of 900 °C has effect on the amount of CO and H_2 that are produced alongside the main product, CO_2 (obtained after H_2O condensation). Increasing the air/fuel ratio leads to an increase in CO_2 concentration. However, H_2 and CO reduces as the air/fuel ratio increases; thereby leading to the production of more CO_2 and H_2O vapour which is condensed to obtain a dry gas composition (Fig. 5). A humid air/fuel ratio of 1.1 was used in the simulation of the CLC–HAT cycle power plant. The trends are consistent with the results reported by Kolbitsch et al. [18].

2.4.3. Effect of fuel reactor temperature on gas composition

The temperature is an important parameter in the successful operation of the CLC system. The fuel reactor temperature can be varied at a given air/fuel ratio to investigate the response of CH_4 and CO composition in the reactor. The fuel reactor temperature is varied between 800 °C and 1000 °C. It was observed that CO concentration decreases rapidly with increasing temperature. CH_4 concentration also decreases slightly at increasing temperature. However, it is observed (Fig. 6) that beyond 900 °C the change in CH_4 concentration is insignificant or fairly constant. This is probably due to weakening of the reactivity of the oxygen carrier particle at a higher temperature.

The results show reasonable accuracy with the results reported by Kolbitsch et al. [18]. Hence, operating the CLC reactors at appropriate temperature (i.e. 850 °C) is essential to improving its rate of reaction and also maintains the carrier particle reactivity.

2.4.4. Effect of fuel flow on Ni solid product

The effect of the fuel flow rate on the solids product is shown in Fig. 7. Increasing the fuel flow rate in the reducer, results in a corresponding increase in the flow rate of Ni to be used in the oxidation reaction. However, Fig. 7 shows that NiO conversion in the fuel reactor is limited by the stoichiometric fuel flow (1 kg/s) available for reduction process. Increasing the flow rate of the fuel after this point does not influence the NiO conversion.

2.4.5. Effect of reducer inlet temperature on gas product yield

Increasing the reducer inlet temperature leads to an increase in the fraction of the CO and H_2, and reduction in the yield of CO_2 in the fuel reactor outlet. It is clear from Fig. 8 that the NiO/Ni carrier particle can convert as much as 99% of the available CH_4–CO_2 below 900 °C. However, less CH_4 is converted to CO_2 at higher temperatures (e.g. 87.3% at 1200 °C). Hence, the fuel reactor temperature is operated at a desirable value within 500–850 °C.

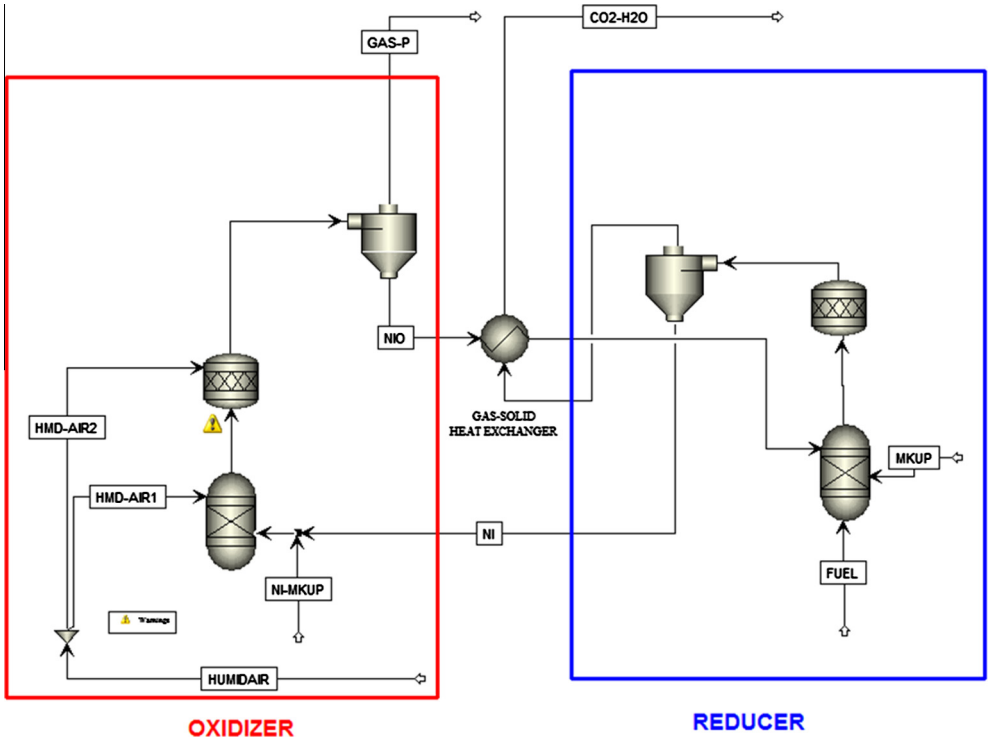

Fig. 3. Simulation of dual CFB for CLC system in Aspen Plus®.

Table 4
Simulation results with the inputs in Table 3.

Components	Mass flow (kg/s)	vol% (gas)	wt.% (solids)
Oxidizer (exhaust)			
N_2	38.32	99.87	–
O_2	0.023	0.13	–
Ni	1.49	–	4.58
NiO	11.33	–	34.81
$NiAl_2O_4$	19.73	–	60.61
Reducer (exhaust)			
CH_4	0.0004	0.01	–
CO_2	2.0728	90.97	–
CO	0.0288	2.19	–
H_2	0.0063	6.83	–
Ni	15.83	–	42.73
NiO	1.49	–	4.02
$NiAl_2O_4$	19.73	–	53.25

The simulation results agree reasonably well (within 10% relative error) with the experimental results reported in Mattisson et al. [29].

3. Simulation of the HAT cycles

3.1. Simulation of conventional HAT cycle in Aspen Plus®

The conventional HAT cycle is an improvement to the combined cycles for its high thermal efficiency. In this cycle, air is compressed in a multistage compressor and intercooled with water, it is then admitted into the saturator where hot water is allowed to evaporate and mix with air. The humidified air is then pre-heated in the recuperator by the exhaust gas from the turbine before it is sent into the combustion unit. The heat recovery is completed with the economizer used to heat water, using the hot exhaust gas from the turbine before being purged in the stack stream [30].

The conventional HAT process simulation is largely based on the parameters from the final reports on advanced fossil fuel power system comparative study by NETL [31]. The HAT cycle power plant used in this study is a simplified model as shown in Fig. 9 [30]. The Aspen Plus® simulation of the plant is shown in Fig. 10. Air is compressed in a multistage compressor with inbuilt intercooler before it enters into the saturator (SEP) where hot water is allowed to evaporate and mix with the air. The humidified air is pre-heated in the recuperator (HEATX) by the exhaust gas from the turbine (EXPANDER) before it is sent into the combustor (RGIBBS), where the fuel reacts with the humidified air to produce the combustion products (i.e. CO, CO_2, H_2O, NO*x*, N_2, etc.). The heat recovery is completed with the economizer (HEATX) used to heat water, using the hot exhaust gas from the turbine before being purged. This approach results in elimination of the HRSG/steam cycle of the NGCC and replaces it with the heat exchangers.

3.2. Simulation of CLC–HAT power cycle in Aspen Plus®

The process flow diagram of the CLC–HAT process is shown in Fig. 11. In this process, methane (CH_4) at 25 °C and 20 bar is pre-heated by the exhaust gas from gas turbine, GT-2 to increase its temperature to 530 °C at 19 bar before it is then admitted into the reducer.

In the reducer, NiO particles are passed by gravity (through the top) into the reducer from the oxidizer. NiO is reduced by the endothermic reaction of CH_4 and NiO to produce Ni, CO_2, and H_2O vapour. The Ni produced serves as the feed into the oxidizer. The product gas discharged from the reducer (stream G-RED) is mainly CO_2 and H_2O vapour. This exhaust gas is used to drive the gas turbine, GT-2 to generate electricity. It is subsequently cooled by releasing heat to methane (CH_4 stream) and process water. CO_2 and water vapour is condensed, CO_2 at 70 °C and 1.1 bar is captured, compressed to a pressure of 150 bar for sequestration.

Table 5
Results to validate CLC simulation in Aspen Plus.

Temperature (°C)	Parameter	Experimental [29]	Simulation	Relative error (%)
700	CO_2 yield (%)	97.88	96.23	1.69
	CO concentration (vol%)	2.0	2.19	9.5
	H_2 concentration (vol%)	6.2	6.83	10.16
800	CO_2 yield (vol%)	96.68	94.92	1.82
	CO concentration (vol%)	3.1	3.41	10.0
	H_2 concentration (vol%)	6.6	7.22	9.39
900	CO_2 yield (vol%)	95.16	91.46	3.89
	CO concentration (vol%)	4.5	4.87	8.22
	H_2concentration (vol%)	7.0	7.61	8.71
1000	CO_2yield (vol%)	93.43	89.87	3.81
	CO concentration (vol%)	6.1	6.49	6.39
	H_2 concentration (vol%)	7.4	8.12	9.72
1100	CO_2 yield (vol%)	91.46	88.49	3.25
	CO concentration (vol%)	7.9	8.72	10.38
	H_2 concentration (vol%)	7.8	8.51	9.10
1200	CO_2 yield (vol%)	89.40	87.23	2.43
	CO concentration (vol%)	9.7	10.26	5.77
	H_2 concentration (vol%)	8.2	9.03	10.12

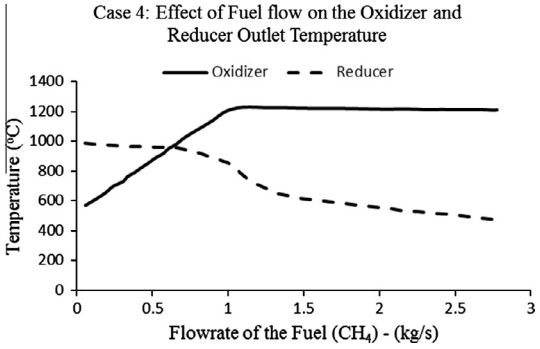

Fig. 4. Effect of fuel flow on temperature change.

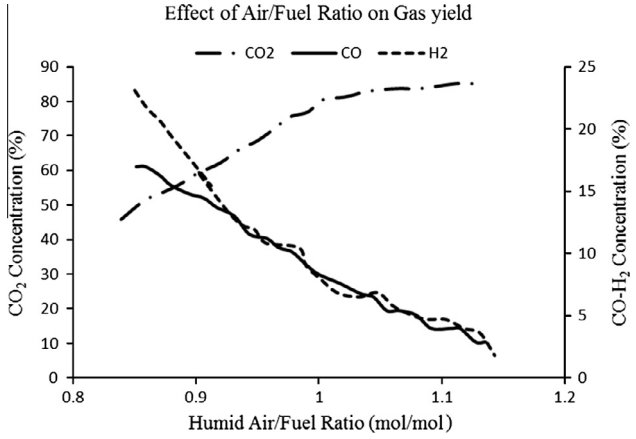

Fig. 5. Effect of humid air/fuel ratio on the gas product distribution.

Furthermore, air at 25 °C and 1 bar is compressed in a multi-stage compressor with intercoolers (COMPR-1) to 20 bar. The compressors are cooled by process water, leading to a temperature increase of 186 °C, required in the saturator. The compressed air is saturated with the heated water to produce a humidified air at 142 °C and 19 bar (with H_2O vapour as a 25 wt.% fraction). The humidified air is then further heated to a temperature of 530 °C by the exhaust gas from GT-1 before it enters into the oxidation reactor.

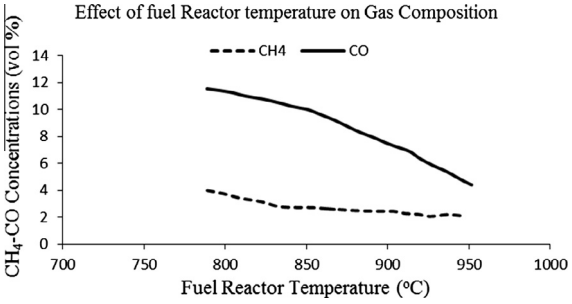

Fig. 6. Effect of fuel reactor inlet temperature on gas composition.

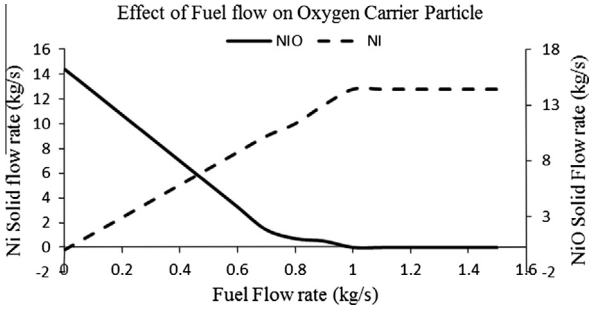

Fig. 7. Effect of fuel flow rate on solids Ni production.

In the oxidizer, Ni is sent from the reducer to be oxidized by the humidified air to form NiO. The oxidation reaction is exothermic, producing an exhaust gas stream (G-OX) at 1200 °C which is passed into turbine GT-1 to generate electricity, pre-heat the humidified air in the HEX-3, and further cooled in HEX-4 and HEX-5 by releasing heat to the process water. The H_2O vapour is then condensed in condenser (GT1-COND) and recovered for re-use. The exhaust gas stream mainly N_2 and water vapour is also condensed in GT2-COND.

3.3. Comparison of the CLC–HAT cycle simulation

The model for the conventional HAT and the CLC–HAT cycles were compared using the simulation results from [9]. The simulation results were compared with this reference case (50 MW_{th}

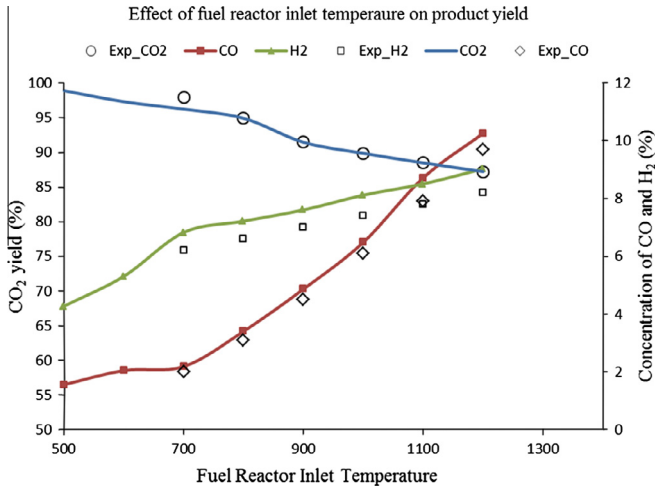

Fig. 8. Effect of reducer temperature on product yield (in comparison with experimental study by Mattisson et al. [29]).

Plant) as shown in Table 5 based on key process performance variables. An inspection of the results presented in Table 5 shows that the model is a good representation of the reference case. Thermal efficiency of the power plant is computed as follows and compared with the reference case.

Thermal efficiency (neglecting pump work)

$$\eta_{th} = \frac{P_{GT} - W_{comp}}{Q_{fuel}} \quad (5)$$

$$Q_{fuel} = \text{fuel burn rate}\left(\frac{kg}{s}\right) \times \text{NCV}\left(\frac{MJ}{kg}\right) \quad (6)$$

where P_{GT}, gas turbine power output from GT-1 and GT-2; Q_{fuel}, chemical energy of fuel (CH_4) = 50 MW_{th} (LHV); W_{comp}, compressor work; NCV, net calorific value.

The energy penalty (fractional reduction in power output per unit of fuel), expressed in fractions or percentage and efficiency penalty (absolute difference between the two process, expressed in % point) as a result of the CO_2 capture and compression is evaluated as shown in Eqs. (7) and (8) [32] and compared with the reference case. In general, the validation results (Table 5) show that the simulation gives a good prediction of the performance of the CLC–HAT cycle when compared to that obtained by [9].

$$\text{Efficiency Penalty} = \eta_{conv} - \eta_{ccs}\ (\%\text{point}) \quad (7)$$

$$\text{Energy Penalty} = \frac{\eta_{conv} - \eta_{ccs}}{\eta_{conv}} \quad (8)$$

η_{conv}, efficiency of the HAT cycle; η_{ccs}, efficiency of the CLC–HAT cycle.

The results in Table 6 shows that the energy penalty and the efficiency penalty of incorporating a CLC CO_2 capture into the system only led to a small parasitic loss of about 3% and 2% respectively. This is a very low penalty level compared to other CO_2 capture approaches.

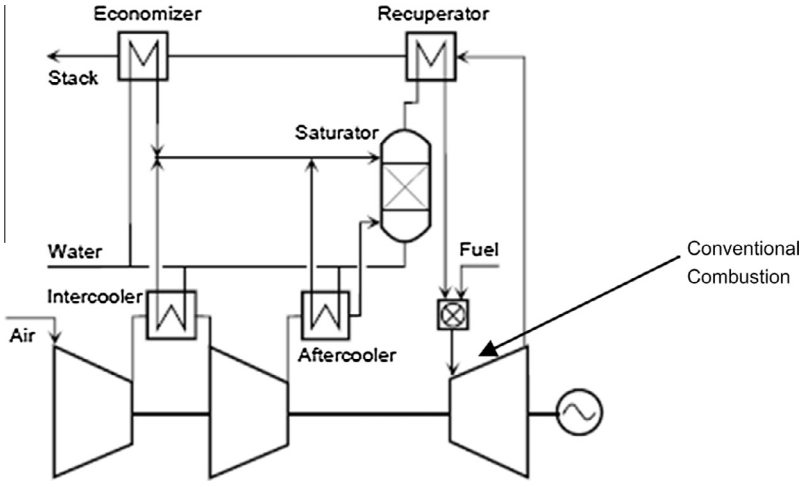

Fig. 9. The conventional HAT cycle flowsheet (adapted from [30]).

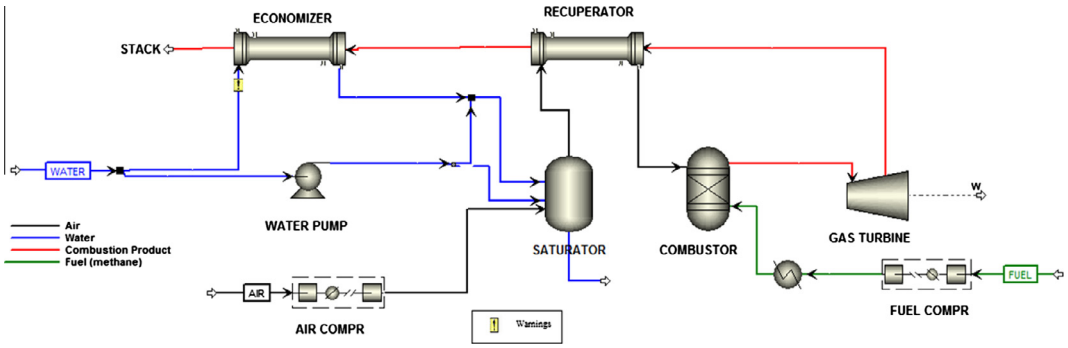

Fig. 10. Simulation of conventional HAT cycle in Aspen Plus®.

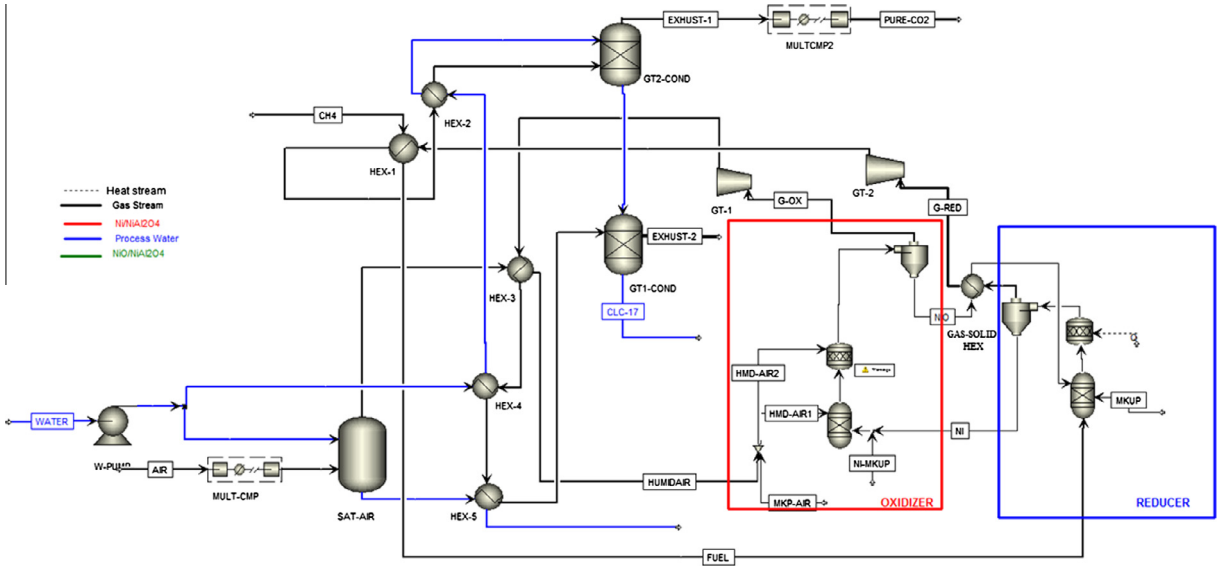

Fig. 11. Simulation of CLC–HAT power cycle in Aspen Plus®.

Table 6
Comparison of simulation results of HAT cycle and the CLC–HAT cycle.

Parameters	Reference case [9]	Conventional HAT	CLC–HAT
Gas turbine (MW_{th})	50.0	43.64	49.02
Compressor work (MW_{th})	22.0	14.14	20.47
Net power (MW_{th})	28.0	29.50	28.55
Net plant efficiency (% LHV)	55.9	59.0	57.1
Energy penalty	3.62	–	3.39
Efficiency penalty (%)	2.1	–	1.9

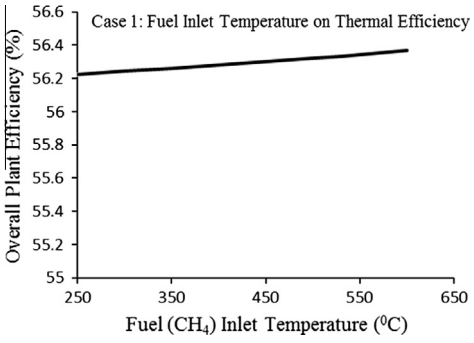

Fig. 12. Effect of fuel inlet temperature.

3.4. Process analysis of the CLC–HAT cycle

The Aspen Plus model was employed to investigate the effect of some key process parameters on the power produced and overall thermal efficiency. The parameters include oxidation (air reactor) and reduction (fuel reactor) inlet and outlet temperatures, mass ratio of humid air to the oxygen carrier (air/Ni–$NiAl_2O_4$ in kg/kg) in the oxidizer, and turbines GT-1 and GT-2 inlet temperatures. Four different cases were considered at varying conditions for the identified process parameters.

3.4.1. Effects of fuel inlet temperature on thermal efficiency

At the given fuel flow and outlet conditions, reducing the fuel inlet temperature means more of the heat from the fuel pre-heat exchanger (HEX-1 in Fig. 11) can be available to the air pre-heat exchanger, thereby increasing the inlet temperature of the oxidizer. In terms of mass flows, the amount of fuel intake in the process is much lower than the air flow requirement in the system. Consequently, little effect is observed on the overall plant efficiency, for example in Fig. 12, an efficiency increase of 0.2% is observed over a temperature range of (250–600 °C). Hence, maximum temperature allowable by ΔT_{min} required in the heat exchanger HEX-1 was used in the simulation to avoid temperature crossing (which indicates a negative driving force for heat transfer between the hot and cold fluids) due to the hot stream outlet temperature lower than the desired cold stream outlet temperature in a counter-current flow arrangement. The trends are consistent with the results reported by Brandvoll and Bolland [9].

3.4.2. Effects of inlet and outlet temperature of oxidizer on efficiency

Assuming constant fuel input, increasing the humid-air temperature at oxidizer inlet influences the power output of the gas turbine GT-1. An increase in the overall efficiency is observed due to a relatively larger increment in the gas turbine output as the oxidizer inlet temperature is increased. The impact of the oxidizer inlet temperature on efficiency is more significant than the fuel reactor inlet temperature – about 7% over the temperature range 400–600 °C. The temperature is set as high as possible limited by the (ΔT_{min}) minimum temperature difference required in the preheat exchanger HEX-3.

From Fig. 13(b), increasing the oxidizer outlet temperature, instantly results in a proportional increase in the power output from GT-1 and the thermal efficiency. The turbine GT-1 outlet temperature also increases and more energy is available for air preheating in HEX-3. These results are consistent with the results reported by Brandvoll and Bolland [9] as shown in Fig. 13(a) and (b).

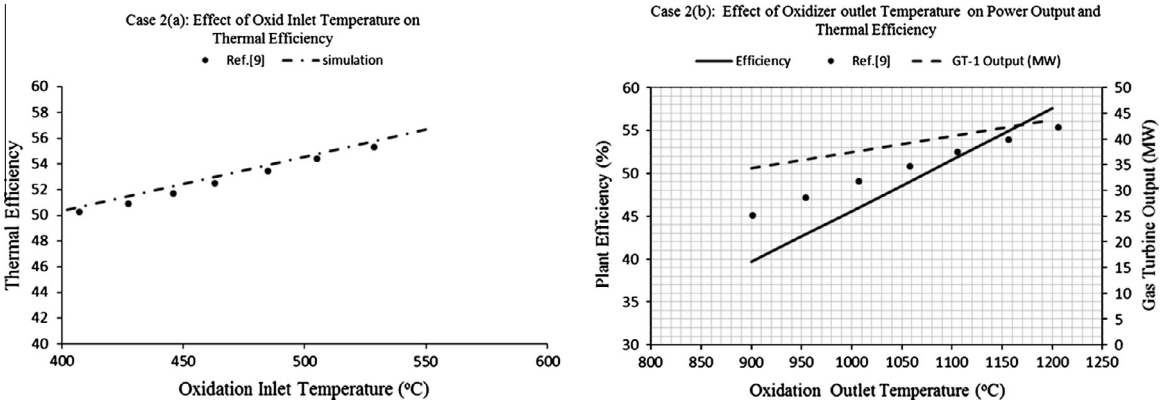

Fig. 13. Effect of (a) oxidizer inlet temperature and (b) oxidizer outlet temperature on efficiency.

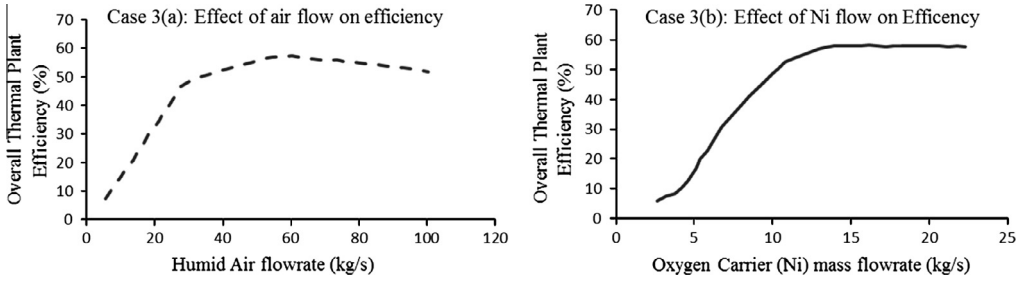

Fig. 14. Effect of (a) humid air flow rate and (b) oxygen carrier on efficiency.

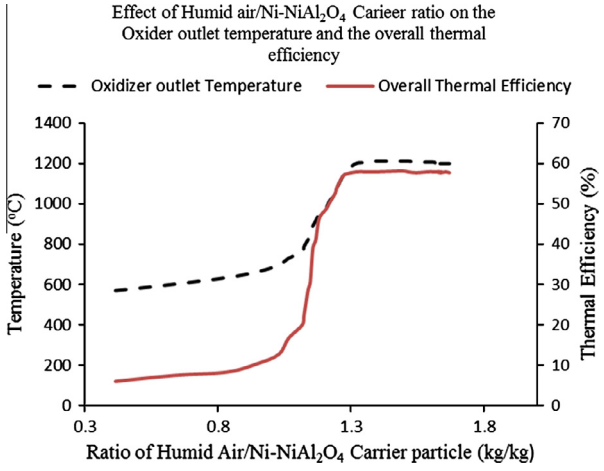

Fig. 15. Effect of air/Ni ratio on temperature and efficiency.

3.4.3. Effect of humid air and Ni flow rate on overall thermal efficiency

Fig. 14(a) shows the effect of humid air mass flow rate on the thermal efficiency of the CLC–HAT cycle. In this present study, 35.6 kg/s of incoming Ni are completely oxidized by 49.8 kg/s of the air. Based on the stoichiometry of the reaction (reaction 7 in Table 2), the air to incoming Ni mass ratio is 1.4. At this point, the oxidation reaction temperature is at maximum value (about 1200 °C, Fig. 15). The thermal efficiency of the plant increases with an increase in the air flow rate due to increase in high temperature working fluid (mainly N_2) at the exit of the oxidation reactor for the gas turbine GT-1. Further increase in air flow rate beyond the stoichiometric amount, the thermal efficiency begins to decrease (Fig. 14(a)). This is due to significant drop in the turbine GT-1 inlet temperature at higher air flow rate.

Fig. 14(b) shows the effect of oxygen carrier (Ni) mass flow rate on the thermal efficiency of the plant. The result shows that the thermal efficiency of the CLC–HAT cycle increases with an increase in the oxygen carrier mass flow rate due to the increase rate of reactions in the reactor and exothermic heat. However, the increase is only up to the stoichiometric amount of Ni required in the reactor. Further increase in the Ni mass flow has no significant impact on the efficiency (Fig. 14(b)). Though, more Ni can still be oxidized by the presence of excess air, this reaction is however limited by the reduction process and its ability to reduce the NiO–Ni.

3.4.4. Effect of air/oxygen carrier ratio on efficiency and oxidizer outlet temperature

The ratio of air to Ni in the oxidizer affects the oxidizer outlet temperature and the overall thermal efficiency of the plant. As described separately in cases 3(a) and (b), increasing the air flow and the oxygen carrier flow rate independently influences the efficiency of the plant (Fig. 3). Increase in the air/Ni mass ratio results in corresponding increase in the thermal efficiency and the oxidizer outlet temperature (Fig. 15), up until the stoichiometric amount. Further increase beyond this point results in no significant change in the temperature and the overall thermal efficiency of the plant.

4. Economic analysis of conventional and CLC–HAT cycles

The main aim of embarking on the CLC–HAT power generation system is to comply with growing demands for CO_2 emission reduction to safeguard the environment from the threat of greenhouse gases and climate change; as well as generate electricity at a high efficiency, as well as reasonably low cost. This section presents economic analysis of CLC power generation system, with CO_2 capture and compression.

Table 7
Basic parameters for economic analysis [33].

Item	Specification	Price/unit
Raw materials		
Methane		2p/kW h
Nickel oxide		11.01 (£/kg)
Process water		£0.37/m. tonne
Utilities		
Cooling water	1 bar, 25 °C	£0.0012/L
Electricity		£0.0775/ kW h
Plant type	Grass roots/clear field	
Depreciation model	5% Per period	
Taxes	20% Per period	
Rate of return	15% Per period	
General and administrative (G and A) expenses	8% Per period	

Table 8
Aspen Icarus® estimate of process equipment cost.

Item	HAT (£)	CLC–HAT (£)
Plant capacity (MW_{th})	50	50
Heaters/heat HEXs (total)	141,200	152,500
Pumps (total)	30,700	85,100
Reactor 1 (Oxidizer)	–	142,700
Reactor 2 (Reducer)	–	142,700
Saturator (sep)	59,600	59,600
Compressors	2,332,000	11,467,300
Gas turbines (total)	8,724,800	12,312,000
Combustor	191,100	–
Total equipment cost	11,479,400	24,361,900
Total direct cost	12,687,300	26,785,600
Fixed capital cost	25,377,700	45,211,800
Working capital	1,332,330	2,260,590
Start up and validation cost	2,537,770	4,521,180
Total capital investment	29,271,400	51,999,270

It is not intended to obtain absolute power generation costs from this evaluation as the results of this work may not accurately reflect the final cost of constructing the plants, but it is a useful method for establishing economic viability of a process and comparing competing processes and for identifying possible bottlenecks.

The following assumptions were used to develop the economic model in the Aspen economic analyser®:

- The proposed plant location for both cases is the United Kingdom (UK).
- The plant is designed to have the capacity to process 1.0 kg/s (50 MW_{th}) of fuel.
- 8000 Working hours per year was used.
- All the cost estimations are carried out in British pounds (£).
- The lifetime of the power plants were set at 30 years.

Table 7 shows the costs of the raw materials and utilities associated with the power cycles. The raw material prices are the general market prices as at June 2011. The amounts of oxygen carriers used were not calculated based on an hourly basis since they are either fixed in the reactors or recycled, and hence it is assumed that the catalysts are changed based on their average lifetimes [4]. Equipment sizes are estimated based on the Aspen Plus® simulations.

The two HAT power cycles were evaluated based on the total capital investment, total manufacturing costs, pay-out period, profitability, internal rate of return and the net present value. A breakdown of the cost of the process equipment for the two options and their associated costs is presented in Table 8. The total operating costs for the conventional and CLC–HAT cycles are presented in Table 10.

Table 9
Estimation of CO_2 emission tax for the conventional HAT cycle.

Parameters	Conventional HAT cycle
Plant generation capacity (MW_{th})	29.50
Carbon price (£/tCO_2)	30.00
CO_2 emission (kg/MW-h)	394.77
CO_2 emission cost (£/year)	3,018,569.33
Plant operating cost (£/year)	4,915,990.00
Total operating cost (£/year)[a]	7,934,559.33

[a] Including annual cost of CO_2 emission tax.

Table 10
Economic indicators for the conventional HAT and CLC–HAT cycles.

	HAT	CLC–HAT
Plant generation capacity (MW_{th})	29.50	28.55
Total capital investment (£)	29,271,400	51,999,270
Raw material cost (£/year)	8,000,000	11,062,634
Total operating cost (£/year)	7,934,559.33	9,104,170.00
Payback period (years)	7.03	6.14
Profitability index (PI)	1.42	1.60
Net present value (NPV) (£)	94,162,100	104,240,000
Internal rate of return (IRR) (%)	26.83	37.87
Capital requirement (£/kW)	584.43	1039.99

The profitability index (PI) shows the relative profitability of any project. For each period, this number is computed by dividing the present value of the cumulative cash inflows by the present value of the cumulative cash outflows. If the profitability index is greater than one, then the project appears to be profitable. If this index is less than one, then the project appears not to be profitable. If this number equals zero then the project incurs no losses or gains (break-even point) [33]. It shows the present value of the benefits relative to the present value of the costs. Table 8 shows the PI of the conventional HAT and CLC–HAT power plant. It can be seen that for every £1 invested in this technology, the total value created by the CLC–HAT cycle is £1.6 as against £1.42 for the conventional cycle.

Mathematically,

$$\text{Profitability Index (PI)} = \frac{\text{Net present value (NPV) of future cash flow}}{\text{Initial investment required}}.$$

4.1. Economic indicators for the conventional and CLC–HAT cycles

Table 10 is a summary of the important economic indicators showing the feasibility of the CLC–HAT technology in comparison to the conventional HAT approach. From the table, it can be seen that the two HAT cycle processes have total capital requirement of power generation of £584/kW_{th} and £1040/kW_{th} with the conventional HAT cycle having the lower value. Nevertheless, the CO_2 emitted in the conventional cycle when quantified and charged at appropriate tax rate (£30/t CO_2 as presented in Table 9) makes the CLC–HAT cycle a more viable option over the life cycle of the plants. The uncertainties in the tax rate due to government policies [34] also means that the cost of operating the conventional plant will increase if the government implements its plan to increase the carbon tax in order to meet the carbon emission reduction target (CERT) of reducing emission to 80% below the 1990 level by 2050 [35]. In the present analysis, an average value of

£30/t CO_2 emitted (which covers the rate between January 2006 to January 2013 [34]) was used to estimate the annual CO_2 emission tax for the conventional HAT cycle.

5. Conclusions

The CLC system with HAT principle shows an efficiency of 57% at oxidizing temperature of 1200 °C and reducer inlet temperature of 530 °C, and a very low penalty point when compared with other CCS options integrated into the power cycles. The sensitivity analysis showed that the overall efficiency of the plant is greatly influenced by the air inlet temperature to the oxidation reactor and its exhaust temperature. The thermal efficiency penalty and thermal energy penalty were found to be very low at a value of 2.0% point and 3.4% point respectively.

The economic evaluation performed shows that the 50 MW_{th} plant with a projected lifetime of 30 years will have a payback period of 7 and 6 years, a net present value of £94.2 million and £104.2 million, and a total capital investment of £29.2 million and £52 million for conventional HAT and CLC–HAT cycles respectively. The profitability index of 1.6 for the CLC as against 1.3 for conventional HAT also affirms the long term superiority of the CLC–HAT cycle in combating CO_2 emission over conventional combustion.

Acknowledgement

This work is financially supported by the Petroleum Technology Development Fund (PTDF), Nigeria.

References

[1] IEA Greenhouse Gas R&D Programme (IEA GHG). Building the cost curves for CO_2 storage, Part 1: sources of CO_2, program report no. PH4/9, July, 2002a, p. 48.
[2] Freund P. Making deep reductions in CO_2 emissions from coal-fired power plant using capture and storage of CO_2. Proc Inst Mech Eng Part A: J Power Energy 2003;217:1–8.
[3] Wang M, Lawal A, Stephenson P, Sidders J, Ramshaw C. Post-combustion CO_2 capture with chemical absorption: a state-of-the-art review. Chem Eng Res Des 2011;89:1609–24.
[4] Fan L-S. Chemical looping systems for fossil energy conversions. New Jersey, USA: John Wiley and Sons; 2010.
[5] Intergovernmental panel on climate change (IPCC). IPCC special report on carbon dioxide capture and storage. Cambridge, United Kingdom and New York, USA: Cambridge University Press; 2005.
[6] Figueroa JD, Fout T, Plasynski S, Mcllvried H, Srivastava RD. Advances in CO_2 capture technology – the U.S. department of energy's carbon sequestration program. Int J Greenhouse Gas Control 2008;2:9–20.
[7] Lu Y, Chen S, Rostam-Abadi M, Varagani R, Chatel-Pelage F, Bose AC. Techno-economic study of the oxy-combustion process for CO_2 capture from coal-fired power plants. In: Paper presented at the annual international pittsburgh coal conference, 2005.
[8] Jin H, Okamoto T, Ishida M. Development of a novel chemical-looping combustion: synthesis of a solid looping material $NiO/NiAl_2O_4$. Ind Eng Chem Res 1999;38:126–32.
[9] Brandvoll O, Bolland O. Inherent CO_2 capture using chemical looping combustion in a natural gas fired power cycle. ASME J Eng Gas Turb Power 2004;126:316–21 [no. 2002-GT-30129].
[10] Johansson E, Mattisson T, Lyngfelt A, Thunman H. Combustion of syngas and natural gas in a 300 W chemical-looping combustor. Chem Eng Res Des 2006;84(A9):819–27.
[11] Jerndal E, Mattisson T, Lyngfelt A. Thermal analysis of chemical-looping combustion. Chem Eng Res Des 2006;84(A9):795–806.
[12] Abad A, Mattison T, Lyngfelt A, Johansson M. The use of iron oxide as oxygen carrier in a chemical looping reactor. Fuel 2007;86:1021–35.
[13] Zhao H, Liu L, Wang B, Xu D, Jiang L, Zheng C. Sol–gel-derived $NiO/NiAl_2O_4$ oxygen carriers for chemical-looping combustion by coal char. Energy Fuels 2008;22:898–905.
[14] Abad A, Adanez J, Cuadrat A, Garcia-Labiano F, Gayan P, de Diego LF. Kinetics of redox reactions of ilmenite for chemical-looping combustion. Chem Eng Sci 2011;66:689–702.
[15] Mendiara T, Garcia-Labiano F, Gayan P, Abad A, de Diego LF, Adanez J. Evaluation of the use of different coals in chemical looping combustion using a bauxite waste as oxygen-carrier. Fuel 2013;106:57–69.
[16] Mattisson T, Jerndal E, Linderholm C, Lyngfelt A. Reactivity of a spray-dried $NiO/NiAl_2O_4$ oxygen carrier for chemical-looping combustion. Chem Eng Sci 2011;66(20):4636–44.
[17] Lyngfelt A, Leckner B, Mattisson T. A fluidized-bed combustion process with inherent CO_2 separation; application of chemical-looping combustion. Chem Eng Sci 2001;56:3101–13.
[18] Kolbitsch P, Proll T, Hofbauer H. Modelling of a 120 kW chemical looping combustion reactor system using Ni-based oxygen carrier. Chem Eng Sci 2009;64:99–108.
[19] Marx K, Bolhar-Nordenkampf J, Proll T, Hofbauer H. Chemical looping combustion for power generation-concept study for a 10 MW_{th} demonstration plant. Int J Greenhouse Gas Control 2011;5(5):1199–205.
[20] Cuadrat A, Abad A, Gayan P, de Diego L, Garcia-Labiano F, Adanez J. Theoretical approach to CLC performance with solid fuels: optimizing the solids inventory. Fuel 2012;97:536–51.
[21] Anheden M, Näsholm AS, Svedberg G. Chemical-looping combustion – efficient conversion of chemical energy in fuels into work. Intersoc Energy Convers Eng Conf 1995;30:75–81.
[22] Wolf J, Anheden M, Yan J. Performance of power generation processes with chemical looping combustion for CO_2 removal – requirements for the oxidation and reduction reactors. In: Proceedings of international Pittsburgh coal conference, Newcastle, New South Wales, Australia, 2001.
[23] Naqvi R, Bolland O, Brandvoll O, Helle K. Chemical looping combustion, analysis of natural gas fired power cycle with inherent CO_2 capture. In: Proceedings of ASME turbo expo 2004, GT2004-53359, Vienna, Austria, June 2004, p. 14–7.
[24] Ishida M, Jin H. A new advanced power-generation system using chemical-looping combustion. Energy 1994;19(4):415–22.
[25] Gallo WLR. A comparison between the hat cycle and other gas-turbine based cycles: efficiency, specific power and water consumption. Energy Convers Manage 1997;38(15–17):1595–604.
[26] Ishida M, Yamamoto M, Ohba T. Experimental results of chemical-looping combustion with $NiO/NiAl_2O_4$ particle circulation at 1200 °C. Energy Convers Manage 2002;43:1469–78.
[27] Iluita I, Tahoces R, Patience GS. Chemical looping combustion process: kinetics and mathematical modelling, American institute of chemical engineers. AIChE J 2010;56(4):1063–79.
[28] Gharebaagh RS, Legros R, Chaouki J, Paris J. Simulation of circulating fluidized bed reactors using Aspen Plus. Fuel 1998;77:327–37.
[29] Mattisson T, Johansson M, Lyngfelt A. The use of NiO as an oxygen carrier in chemical looping-combustion. Fuel 2006;85:736–47.
[30] Korobitsyn MA. New and advanced energy conversion technologies: analysis of cogeneration, combined and integrated cycles. PhD Thesis, thermal engineering department, University of Twente, Netherlands, 1998.
[31] Parsons EL, Shelton WW. Advanced fossil power systems comparison study, Final Report, National Energy Technology Laboratory, Pittsburgh, PA, 2002.
[32] Maurstad O. An overview of coal based integrated gasification combined cycle (IGCC) technology. Cambridge, MA: Massachusetts Institute of Technology, Laboratory for Energy and the Environment; 2005. Publication No LFEE 2005-002 WP.
[33] Aspen Technology. Aspen icarus V7.2 reference guide, icarus evaluation engine (IEE) V7.2, Aspen Technology, Inc, Burlington, MA, 2010b.
[34] Ares E. Carbon price floor: house of commons library standard note, energy and environment section. House of commons library, SN05927, 2013. p. 1–10 <http://www.parliament.uk/briefing-papers/SN05927/carbon-price-floor>.
[35] Watson C, Bolton P. Carbon emission reduction target (CERT): house of commons library standard note, science and environment, social and general statistics section. House of commons library, SN/SC/06196, 2013. p. 1–9 <http://www.parliament.uk/briefing-papers/SN06196/carbon-emissions-reduction-target-cert>.